Nanoscale

MINIREVIEW

View Article Online
View Journal | View Issue

Cite this: *Nanoscale*, 2023, **15**, 18184

Graphene-based biosensors for detecting coronavirus: a brief review

Filimon Hadish Abrha,*[a,b] Tadele Hunde Wondimu,[b,c] Mebrahtu Hagos Kahsay,[d,e] Fetene Fufa Bakare,[b,c] Dinsefa Mensur Andoshe[b] and Jung Yong Kim *[b,c]

Received 11th September 2023,
Accepted 24th October 2023

DOI: 10.1039/d3nr04583h

rsc.li/nanoscale

The coronavirus (SARS-CoV-2) disease has affected the globe with 770 437 327 confirmed cases, including about 6 956 900 deaths, according to the World Health Organization (WHO) as of September 2023. Hence, it is imperative to develop diagnostic technologies, such as a rapid cost-effective SARS-CoV-2 detection method. A typical biosensor enables biomolecule detection with an appropriate transducer by generating a measurable signal from the sample. Graphene can be employed as a component for ultrasensitive and selective biosensors based on its physical, optical, and electrochemical properties. Herein, we briefly review graphene-based electrochemical, field-effect transistor (FET), and surface plasmon biosensors for detecting the SARS-CoV-2 target. In addition, details on the surface modification, immobilization, sensitivity and limit of detection (LOD) of all three sensors with regard to SARS-CoV-2 were reported. Finally, the point-of-care (POC) detection of SARS-CoV-2 using a portable smartphone and a wearable watch is a current topic of interest.

[a]*Department of Chemistry, College of Natural and Computational Sciences, Aksum University, Aksum 1010, Ethiopia*
[b]*Department of Materials Science and Engineering, Adama Science and Technology University, Adama 1888, Ethiopia. E-mail: filimon.hadish@astu.edu.et, jungyong.kim@astu.edu.et*
[c]*Center of Advanced Materials Science and Engineering, Adama Science and Technology University, Adama 1888, Ethiopia*
[d]*Department of Applied Chemistry, College of Natural and Computational Sciences, Mekelle University, Mekelle 231, Ethiopia*
[e]*Department of Applied Chemistry, Adama Science and Technology University, Adama 1888, Ethiopia*

Introduction

The coronavirus (COVID-19) pandemic has infected several billion people, causing over a million deaths worldwide, and the economic fallout has resulted in a global panic.[1] The severe acute respiratory syndrome (SARS)-associated coronavirus pandemic has not only led to an unexpected public health crisis but also severely hampered the global economy, with analysts measuring its detrimental impact compared to

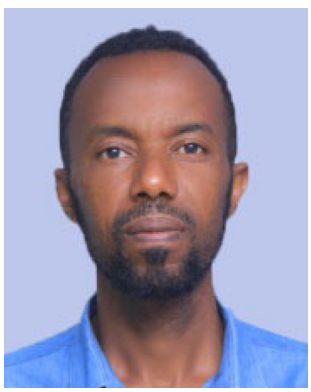

Filimon Hadish Abrha

Dr Filimon Hadish Abrha obtained his Ph.D. degree from the Department of Material Science and Engineering (MSE), National Taiwan University of Science and Technology (NTUST), Taiwan in 2018. Then, he worked as an Assistant Professor in the Department of Chemistry, Axum University, until 2021. From July 2022 to the present, he is serving at the Department of Materials Science and Engineering, Adama Science and Technology University (ASTU) on temporary basis. His research interests are Biosensors, Graphene, 2D Materials, Quantum Dots, Thin Films, Plasma, and Chemical Vapor Deposition (CVD).

Tadele Hunde Wondimu

Dr Tadele Hunde Wondimu is currently an Associate Professor at Adama Science and Technology University (ASTU), Center of Advanced Materials Science and Engineering at the School of Mechanical, Chemical, and Materials Engineering, Ethiopia. He received his PhD from the Department of Materials Science and Engineering at the National Taiwan University of Science and Technology in 2018. He has broad experience in materials design and synthesis for biological applications and various energy storage systems, such as redox flow batteries, fuel cells, solar cells, supercapacitors, water splitting, and electrochemical sensors.

the Second World War.[2] Moreover, it affects birds and mammals[3,4] and usually causes mild respiratory diseases in humans. However, strains have emerged, such as 2002–2004 SARS and Middle East respiratory syndrome (MERS), causing outbreaks of this lethal respiratory disease.[3] The causative agent SARS-CoV-2 indicates coronavirus disease 2019 (COVID-19). In addition to SARS and MERS, swine acute diarrhea syndrome (SADS) harmed thousands of human lives in 2017. SADS agents are known to originate from bats. Its viruses are highly pathogenic to humans and livestock.[5] Therefore, as these rapidly spreading viruses continue to increase, quick diagnostic techniques are critical to reduce and prevent the spread and transmission of these viruses.

Thus far, diagnostic techniques, such as clustered regularly interspaced short palindromic repeats (CRISPR),[6] reverse transcription polymerase chain reaction (RT-PCR), lateral flow assays (LFA), lateral flow immunoassay, and reverse transcription loop-mediated isothermal amplification (RT-LAMP), have been developed as detection methods for COVID-19. Although these methods exhibit superior analytical sensitivity, they have disadvantages because they require skilled personnel to operate complex analytical instruments and they are highly susceptible to other interference materials, resulting in either false positives or false negatives. Moreover, the aforementioned methods are incompatible with point-of-care testing, which poses a challenge to their portability.[7]

To improve these diagnostic methods, real-time, ultrafast, and low-cost sensors have been studied and developed.[8,9] For example, sensors that incorporate nanomaterials, such as carbon nanotubes, multiwall carbon nanotubes, carbon dots, graphene, and transition metal dichalcogenides (TDMs: WS molybdenum disulfide, MoS_2 molybdenum diselenide, WS_2 tungsten disulfide and WSe_2 tungsten diselenide), have been investigated.[10] In particular, the latter nanomaterials have been widely studied owing to their applications in energy storage, catalyst, nanomedicine, optics and electronics.[11] However, most of these materials contain elements that are toxic to the environment and human beings. Among the elements commonly used in the synthesis of MXenes, prolonged exposure to chromium, tungsten, and molybdenum could result in physical, muscular, and neurological degenerative diseases.[12] Although these elements are essential for biochemical and physiological purposes,[13] it would be very difficult to apply them to implantable sensors. This is because excessive ingestion of molybdenum can lead to serious bone and joint deformity, liver and kidney failure, and sterility.[14] Beyond safety precaution synthesis of high quality, continuous, and spatially uniform single-layer TDMs, MXene is a challenging material that poses a large initial resistance[15] unlike graphene, which has been in the limelight of research for over two decades. Therefore, considering the safety, ease of synthesis, bio-functionalization[16–18] and biocompatibility,[19,20] graphene is a well-studied material for detecting coronavirus, among the other nanomaterials.[21]

The biosensor is mainly composed of three parts: the biological detection component, transducer, and processing unit.[22,23] Through this mini-review, we mainly discuss graphene-based biosensors, such as electrochemical, field-effect transistor (FET) and surface plasmon resonance (SPR) sensors (Scheme 1). Notably, although FET could be considered an electrochemical sensor if there is electrochemical doping,[24,25] instead of an electrostatic sensor, we reviewed it separately based on the particular device structure and physics. Beginning with a general overview of the different variants (families of coronavirus), these biosensors are briefly covered, focusing on recent progress along with fabrication processes and the performance of the devices. Finally, we summarize the results accompanying our perspectives.

Mebrahtu Hagos Kahsay

Dr Mebrahtu Hagos Kahsay received his M.Sc. degree in Analytical Chemistry from Addis Ababa University, Ethiopia, in 2011 and his ph.D. degree in Chemistry from Andhra University, India, in 2018. He worked as an Assistant Professor in Analytical Chemistry for various public universities in Ethiopia, namely Woldia University, Adama Science and Technology University, and currently at Mekelle University. His research interest is a green synthesis of nanomaterials for wide applications, including photocatalysis, adsorption, antimicrobial, antifungal and anticancer activities.

Fetene Fufa Bakare

Dr Fetene Fufa Bakare is currently an assistant professor at Adama Science and Technology University (ASTU), Center of Advanced Materials Science and Engineering at the School of Mechanical, Chemical, and Materials Engineering, Ethiopia. He received his PhD from the Department of Materials Science and Engineering at the National Taiwan University of Science and Technology in 2019. He has broad experience in materials design and synthesis for various biological applications, such as bioactive materials and bio-ceramics materials and various energy storage systems, such as fuel cells, solar cells, and super capacitors.

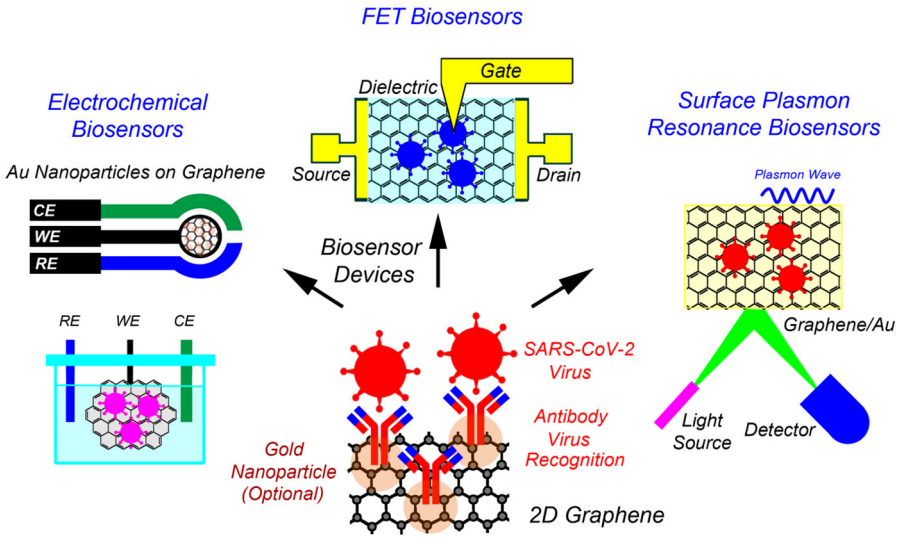

Scheme 1 Schematic overview of graphene-based biosensors: electrochemical, field-effect transistor (FET), and surface plasmon resonance (SPR) sensors. Here, 'WE', 'RE', and 'CE' represent the working electrode, reference electrode, and counter electrode, respectively.

SARS-CoV-2

Thus far, alpha, beta, gamma, delta, and omicron (α, β, δ, γ, and o) variants of coronaviruses that mutate over time were identified.[26] Although a family of the virus belonging to α-/β-variants infects mammals, including humans, the γ-/δ-variants mainly transmit infections to birds. Here, α- and β-variants correspond to severe acute respiratory syndrome coronavirus (SARS-CoV-2) and middle-east respiratory syndrome coronavirus (MERS-CoV), respectively. Specifically, SARS-CoV-2 belongs to the nidovirales family of coronaviridae, resulting in the main cause of mortality.[27] As shown in Fig. 1a, the structure of SARS-CoV-2 is composed of nucleocapsid (*N*), membrane (*M*), envelope (*E*), ssRNA (+), and spikes (*S*1 & *S*2), among which the protein spikes serve as a binding site and fuse to the host cell receptor.[28] Here, the SARS-CoV-2 name itself is known to originate from the typical spike (*S*) proteins that are ~20 nm long and scarcely embedded in the lipid bilayer membrane. The epitope or antigenic determinant is a group of amino acids or other chemical groups[29,30] known as the receptor-binding domain (RBD) and receptor-binding motif (RBM) of SARS-CoV-2. They stay on top of the *S* proteins with 25 nm space apart and enable the virus to interact with the angiotensin converting enzyme 2 (ACE2) receptor of the host cell.[31] Specifically, RBD serves as the primary target antigen for neutralizing antibodies.[32]

Dinsefa Mensur Andoshe

Dr Dinsefa Mensur Andoshe is an associate professor at Adama Science and Technology University (ASTU), Department of Materials Science and Engineering. He obtained a diploma in Physics from Hawassa College of Teacher Education in 2004, a BSc degree in Physics from Jimma University in 2008, and an MSc. in Materials Science in 2012 from Hawassa University. He completed a Ph.D. in 2017 in Materials Science and Engineering at Seoul National University, Korea. Moreover, Dr Dinsefa served as the founder department staff team of the Materials Science and Engineering of Adama Science and Technology University.

Jung Yong Kim

Prof. Jung Yong Kim received his PhD in Chemical and Biomolecular Engineering from the Korea Advanced Institute of Science and Technology (KAIST) in February 2004. He has worked at Samsung Electronics, the University of Texas at Austin (Prof. Allen J. Bard), the University of Minnesota-Twin Cities (Prof. C. Daniel Frisbie), and Linköping University (Prof. Olle Inganäs). Currently, he is a professor of Materials Science and Engineering and the director of the Center of Advanced Materials Science & Engineering at Adama Science and Technology University. His research focuses on Polymer and Perovskite Semiconductors for Electronics, Optoelectronics and Bioelectronics.

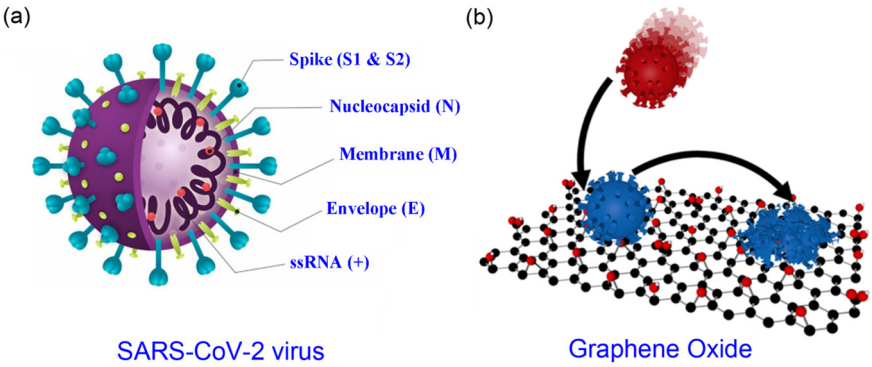

Fig. 1 (a) Schematic of the SARS-CoV-2 virus structure.[28] (b) Immobilization of SARS-CoV-2 at the functionalized GO surface, subsequently followed by reduction of *S* and *N* proteins of SARS-CoV-2 virus (reprinted with permission;[35] Copyright © 2021, American Chemical Society).

Mutation of SARS-CoV-2 to a different variant is induced in its spike proteins, occurring mostly in the RBD part. The mutation allows the virus to remain immune to different vaccination trials for a significant time.[33,34] However, the epitope sitting on the spike S protein is a large group of amino acids. Whether these amino acids belong to primary, secondary or tertiary structures, their terminal chemical compounds are rich in amide, carboxyl, amine, sulfide, and many other functional groups. These moieties are known to be favorable for sharing electrons through covalent bonds with the functionalized graphene surface. This indicates that SARS-CoV-2 can be easily detected in graphene-based biosensors. However, the bio-functionalization process (specific antibody attachment) on top of the 2D-graphene surface should be helpful for high-accuracy SARS-CoV-2 viral target biosensor applications through antibody–antigen complex formation, resulting in high sensitivity and selectivity.

Graphene and graphene oxide

Graphene is a 2D honeycomb crystal lattice with sp^2p_z hybridized carbon, which contains two atoms per unit cell. Here, the electrons in sp^2 orbital form three covalent σ-bonds although the π-electrons in p_z-orbitals are non-bonded and delocalized in a single flat layer of carbon atoms. Hence, the 2D delocalized π-orbitals show a conical shape in the electronic structure where the conduction and valence bands touch at the *Diract point*, resulting in a zero energy gap.[36,37] Over the past two decades, graphene has played a crucial role in the field of smart materials owing to its unique electrical, optical, thermal, and mechanical properties.[38–43] However, limitations, such as zero bandgap[44] and non-emissive surface,[45] hinder further applications of graphene in the pristine state. Therefore, the surface of graphene has been usually modified through chemical functionalization,[46] substitutional doping,[47–49] microwave irradiation,[50,51] downstream oxygen plasma,[52] hydrothermal method, and liquid exfoliation.[53] In this circumstance, it should be very important to understand the chemical/physical attachment of various atoms and molecules to the surface of the π-conjugated graphene.[54] In the case of non-covalent bonding, such as π-orbital interactions (*e.g.*, π–π, H–π, gas–π, and cation/anion–π), the binding energies could be electrostatic, dispersion, and induction.[18] However, these intermolecular interactions depend on the physical state (*e.g.*, stabilization or destabilization) of the graphene surface, indicating that it is not sustainable but transient. However, the covalent functionalization of graphene surfaces with oxygen is an important chemical approach to surface engineering.[55] For example, graphene oxide (GO) has a versatile surface with functional groups, such as hydroxyl, carboxyl, epoxide, and carbonyl,[56,57] which are useful for the covalent immobilization of bio-receptors.[58,59] Consequently, graphene-based biosensors have been used for detecting glucose (diabetes),[52,60,61] nucleic acid (DNA/RNA),[62–64] and various pathogenic bacteria/viruses.[65–69]

Intermolecular interactions between graphene derivative and SARS-CoV-2

A well-designed graphene surface can have a binding function similar to that of a target molecule. Fukuda *et al.*[35] investigated the antiviral effect of GO nano-sheets on SARS-CoV-2. Here, the plus-charged spikes of the virus were attracted to the minus-charged GO surface. As shown in Fig. 1b, SARS-CoV-2 proteins were decomposed through adsorption and concomitant inactivation on top of the GO surface. Importantly, graphene has a significant capacity to capture viral antibodies to its 2D surface in addition to the aforementioned antibacterial and antiviral properties. Moreover, functionalized graphene can effectively detect a viral-structured protein as a target, enabling a large-scale diagnosis for public health. Accordingly, graphene-based biosensors are suitable for SARS-CoV-2 detection, as emphasized by Yasri and Wiwanitkit.[70] The biofunctionalization of graphene-based devices affords the enhancement of biocompatibility and bio-recognition ability with high sensitivity and selectivity. Therefore, the direct immobilization of the virus on top of the GO or graphene surface clearly highlights the potential of graphene-based SARS-CoV-2 biosensors.

Table 1 Graphene-based COVID-19 detection methods

Graphene modification	Method of detection	Target/analyte	Sample type	LOD	Ref.
PBASE/G/SiO_2/Si	FET	SARS-CoV-2 antigen	Nasopharyngeal swab specimens in UTM	1 and 100 fg mL^{-1}	71
MXene (Ti_2C)/G/SiO_2/Si	FET	SARS-CoV-2 antigen	Artificial saliva and PBS	1 fg mL^{-1}	72
AgGO/SiO_2/Si	FET	SARS-CoV-2 antigen	PBS	2.1×10^{-18} M	73
GO/Pt/PdNp/SiO_2/Si	FET biosensor	SARS-CoV-2 antigen	PBS	1 fg mL^{-1}	74
PBASE/G/SiO_2/Si	Surface plasmon sensor	SARS-CoV-2 antigen	Artificial saliva, buffer	1 and 3.75 fg mL^{-1}	75
PI/LSG/AuNS/Cys/EDC : NHS	Electrochemical biosensor	SARS-CoV-2 antigen	Blood serum in PBS	2.9 ng mL^{-1}	76
Au/Ti/EG/6H-SiC	Electrical transduction	SARS-CoV-2 antigen	Mid-turbinate swabs, saliva and exhaled breath aerosol samples in PBS	1 ag mL^{-1}	77
ZnS/G/GCE	Electrochemical biosensor	SARS-CoV-2 nucleic acids	Hybridized DNA in 1.0 M KCl and 0.2 M $K_3[Fe(CN)_6]$ solutions	2.1×10^{-20} M	78
G/Au/MgF_2	Surface plasmon sensor	Ethyl butanoate in SARS-CoV-2	Exhaled breath	0.0224 RIU	79
PMB/PILs/rGO/AuNPs	Miniature electrochemical biosensor (acupuncher)	SARS-CoV-2	PBS	38 pg mL^{-1}	80
G/paper	Electrochemical biosensor	Anti-SARS-CoV-2 monoclonal antibody CR3022	RBD in PBS	2 fg mL^{-1}	81

PBSAE = 1-pyrenebutyric acid *N*-hydroxysuccinimide ester, G = graphene; MXene = 2D transition-metal carbides; Ti_2C = Di-titanium carbide; SWCNTs = single wall carbon nanotube; PI = polyimide; LSG = laser-scribed graphene; AuNS = gold nanostructures; Cys = cysteamine; EDC = 1-ethyl-3-(3-dimethylaminopropyl) carbodiimide; NHS = *N*-hydroxy succinimide; ZnS = Zinc sulfide; GCE = glassy carbon electrode; PMB = poly methylene blue; PILs = poly ionic liquids, rGO = reduced graphene oxide; AuNPs = gold nanoparticles; RIU = refractive index unit, WS_2 = tungsten disulfide; $KNbO_3$ = potassium niobate; BP = black phosphorus; Blue P = blue phosphorus; UTM = universal transport medium.

Table 1 displays the versatile graphene-based SARS-CoV-2 biosensors using the detection method, sample type, and limit of detection (LOD).

Electrochemical biosensors

Electrochemical biosensors are suitable for ultrasensitive point-of-care (POC) SARS-CoV-2 detection at the time and place of patient care. They are cost-effective and simple for rapid and high-sensitivity detection.[82] Basically, electrochemical sensors rely on the measurement of an electrical signal recorded by an electrochemical transducer. They can be categorized as amperometric, potentiometric, conductometric, and impedimetric depending on the type of signal.[83] These biosensors have been widely used to detect biomaterials, such as nucleic acids, proteins, small molecular antibodies, and viruses.[84]

For instance, Pan and coworkers developed rapid (less than 5 min), ultrasensitive, and quantitative detection of SARS-CoV–2 using an antisense oligonucleotide-directed electrochemical biosensor chip, affording a sensitivity of 231 (copies per μL)$^{-1}$ and LOD of 6.9 copies per μL (Fig. 2). Fig. 2a shows the schematic configuration of the biosensor, targeting viral nucleocapsid phosphoprotein (*N*-gene) using highly specific antisense oligonucleotides (short single-stranded deoxyribonucleic acid; ssDNA) on top of the gold nanoparticle (AuNP)-modified graphene/paper platform. Fig. 2b shows the operation principle of this electrochemical biosensor. First, the infected samples are collected from the nasal swab or saliva of the patients with COVID-19. Second, the viral SARS-CoV-2 ribonucleic acid (RNA) is extracted from the samples. Third, viral RNA is added on top of the ssDNA-AuNP/graphene/paper platform. Fourth, wait 5 min for the incubation time. Finally, the electrical signals (voltage and/or current) are recorded. Fig. 2c shows two kinds of configurations without and with AuNPs on graphene/paper substrate. As shown in Fig. 2d, when AuNPs were employed, the sensing signal (here, the voltage difference) was much stronger, indicating that AuNPs are very useful components of electrochemical biosensors. Fig. 2e shows the positive/negative decision method using the complexation of ssDNA on AuNPs with the viral RNA. Importantly, the sensing signal is also dependent on the particle size of AuNPs, as shown in Fig. 2f, indicating that the large surface area of AuNPs capped with ssDNA (the immobilized recognizing element) is a key factor for the effective sensing of viral RNA.

A resistive model was employed to explain the above sensing platform, in which the change in voltage (ΔV) across the electrochemical sensor chip is given by

$$\begin{aligned}\Delta V &= R\frac{\mathrm{d}q}{\mathrm{d}t} = RQ_{\mathrm{RNA}}S\frac{\mathrm{d}[\mathrm{RD}]_t}{\mathrm{d}t} \\ &= RQ_{\mathrm{RNA}}Sk_{\mathrm{d}}\frac{k_{\mathrm{a}}[D]_{\max}[R]}{k_{\mathrm{a}}[R]+k_{\mathrm{d}}}e^{-k_{\mathrm{d}}t},\end{aligned} \quad (1)$$

where R is resistance, q is charge, t is time, Q_{RNA} is the electrical charge caused by the RNA per surface area, and S is the graphene surface area. Furthermore, $[\mathrm{RD}]_t$ is the surface density of the binding complex between RNA and ssDNA, k_{d} is the

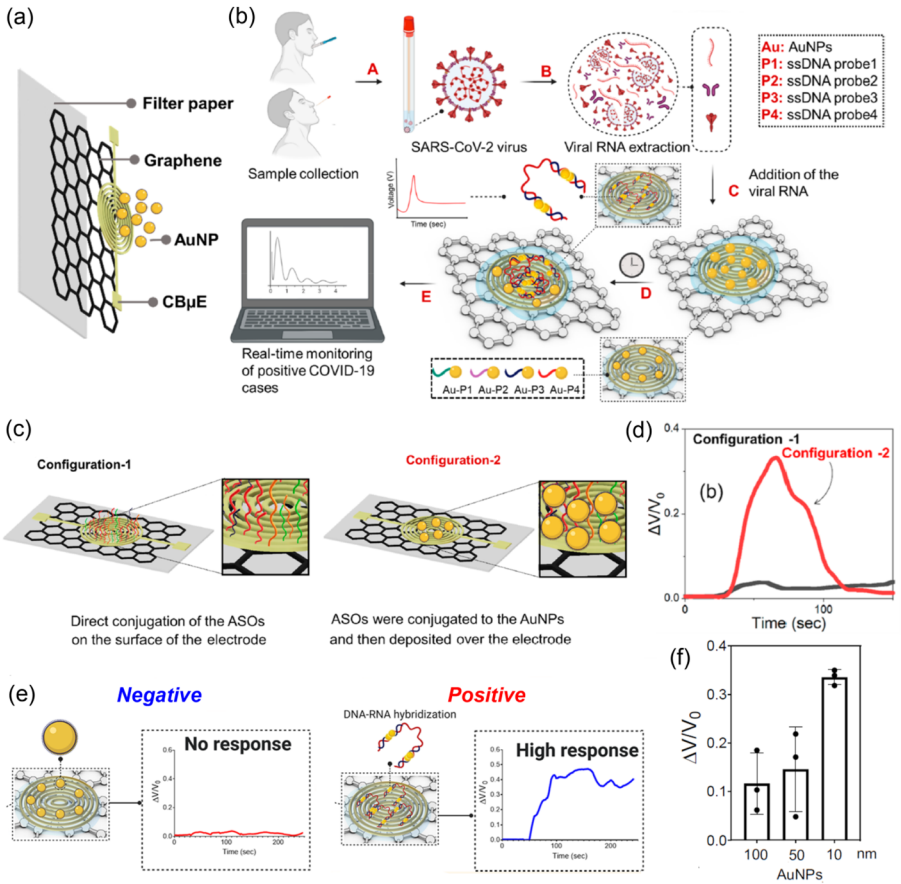

Fig. 2 (a) Structure of the electrochemical biosensor. (b) Operation principle of the electrochemical biosensor. (c) Schematic representation of the proposed concept behind the enhancement in electrochemical response using gold nanoparticles when capped with ssDNA probes. (d) Relative change in the biosensor output voltage for the two sensor configurations. (e) Decision of Covid-19 negative and positive. (f) Sensor output response with varying sizes of functionalized spherical gold nanoparticles. Reprinted with permission from ACS Nano.[85]

dissociate rate constant, k_a is the association rate constant, $[D]_{max}$ is the maximum number of ssDNA probes, and $[R]$ is the concentration of the target RNA. Here, the dissociation to the formation of the RNA-DNA complex is given by $d[RD]_t/dt = k_d[RD]_t$, where $[RD]_t$ is rewritten as $\{k_a[D]_{max}[R]/(k_a[R] + k_d)\}$ $e^{-k_d t}$. The resistor model (eqn (1)) suggests that a high sensitivity of the sensor-chip function could be obtained when more antisense ssDNA (*i.e.*, large $[D]_{max}$ value) are immobilized on the surface of AuNPs (*e.g.*, ~10 nm in diameter) on the graphene/paper substrate.

Recently, the laser-scribed graphene (LSG)-based biosensor has gained significant attention as a miniaturized electrochemical POC immunoassay.[86] Underpinning the evolution, Beduk *et al.*[76] established an LSG biosensor fabricated through the electrodeposited 3-dimensional gold nanostructures (AuNSs) on top of the LSG for detecting SARS-CoV-2. As shown in Fig. 3, this electrochemical immunosensor can be integrated into a smartphone (Fig. 3a) or wearable watch (Fig. 3b), which can provide a user friendly POC diagnostic platform. Specifically, the second-generation custom with the brand name of 'KAUSTat' (Fig. 3a) has a poly-potentiostat device composed of built-in memory, battery, bluetooth, mini-USB connector, SD-card slot, and connectable add-on device, which affords multiple amperometric and voltammetric measurements.[76]

The differential pulse voltammetry (DPV) (Fig. 3c and d) response for various stages of the fabricated electrode showed a significant increase in the oxidation current density by electrodepositing AuNPs and cysteamine onto the LSG electrode. This increase was attributed to the high conductivity (owing to the surface area and catalytic activity of the AuNPs) and the polarizable ammonium groups on the electrode. Although the presence of graphene in the fabricated electrode increases electron transfer, the bulk structures of antibody-analyte (SARS-CoV-2) binding may partially hinder the electron transfer process at the surface of the electrode, leading to a decrease in the oxidation current (Fig. 3c). However, it is notable that the performance of the portable handmade POC potentiostat (Fig. 3d) showed a comparable function compared to the commercially available PalmSens electrochemical workstation (Fig. 3c).

Fig. 3e shows the response of this electrochemical immunosensor in the presence of SARS-CoV-2, IgM/IgG (7 : 3), IgM, IgG/IgM (3 : 7), IgG/IgM, and IgG (p value > 0.05), for which

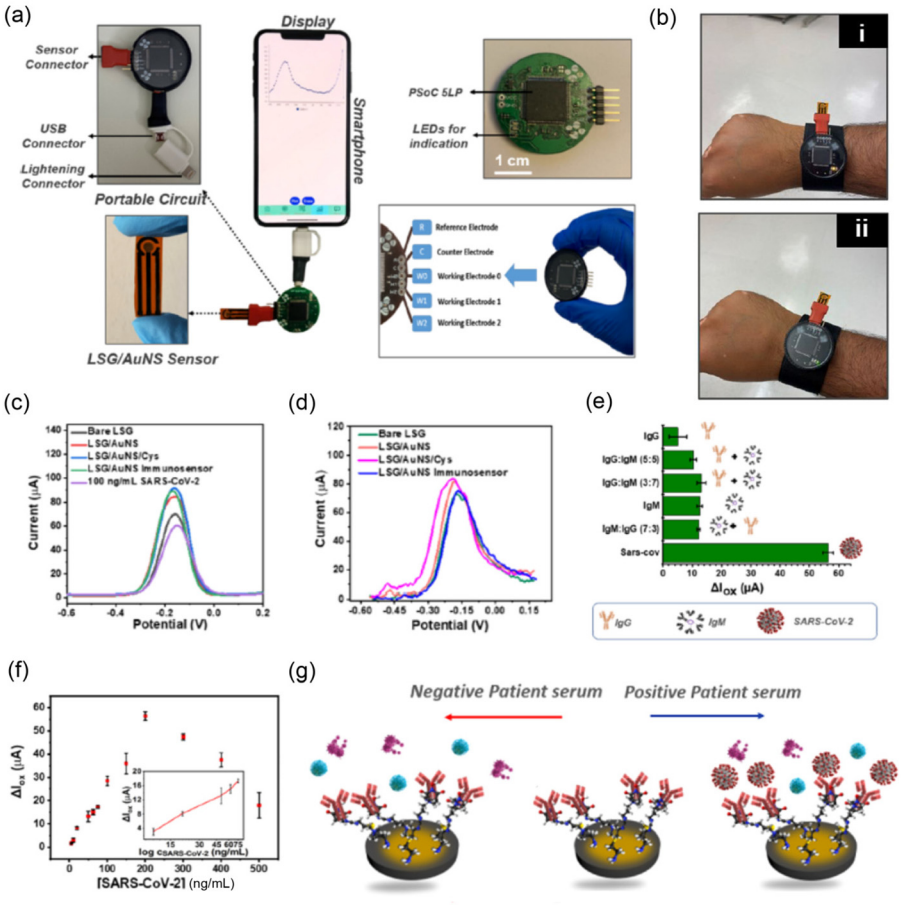

Fig. 3 (a) Portable handmade POC potentiostat connected to a smartphone *via* a USB-C connection to record the signal. (b) Representation of KAUSTat used as a standalone watch-like device showing (i) LED on and (ii) LED off for indication. DPVs of the LSG/AuNS immunosensor presenting ΔI_{ox} (the change in oxidation current) after each experimental step and the measurement of 100 ng mL^{-1} SARS-CoV-2 spike protein by (c) PalmSens potentiostat and (d) portable handmade POC potentiostat. (e) Response of the LSG/AuNS immunosensor in the presence of SARS-CoV-2, IgM/IgG (7 : 3), IgM, IgG/IgM (3 : 7), IgG/IgM, and IgG (p value > 0.05). SARS-CoV-2 protein (150 ng mL^{-1}) and interfering proteins (immunoglobins, IgG and IgM) were used for the selectivity test. (f) Proposed LSG/AuNS immunosensor in response to different concentrations of the SARS-CoV-2 spike protein *vs.* the LSG reference electrode. (g) Representation of SARS-CoV-2 detection in human blood serum. (Reprinted from[76] by the grant of the PMC Open Access Subset from Analytical Chemistry.)

SARS-CoV-2 protein (150 ng mL^{-1}) and interfering proteins (immunoglobins, IgG and IgM) were used for the selectivity test. The electrochemical tests carried out using the DPV method (Fig. 3f) for a wide range of SARS-CoV-2 S1 spike proteins confirmed that the device can detect low concentrations and achieve an LOD of 2.9 ng mL^{-1}, as depicted in the inset in Fig. 5f. Moreover, the clinical RT-PCR positive and negative serum samples at 10 and 25% dilution provided an LOD of 3.8 and 8 ng mL^{-1} as well as 16 and 10 ng mL^{-1}, respectively. Then, the authors suggested that this kind of electrochemical biosensor (see the schematic explanation in Fig. 3g) offers a portable, easy-to-use, and reliable POC diagnostic alternative platform for future applications.[76]

Kim and coworkers[77] reported a real-time ultra-sensitive detection of SARS-CoV-2 using a quasi-free-standing epitaxial graphene-based biosensor. Despite simple and low-cost fabrication techniques, this biosensor can rapidly detect both the mid-turbinate swabs and the exhaled breath aerosol samples of a SARS-CoV-2 infected patient with an LOD of 1 ag mL^{-1} (a spike protein antigen concentration). Interestingly, the potential application of a portable device was demonstrated by a fast response time of 0.6 sec to a human saliva sample in real-time detection. Another competent candidate among the graphene-based SARS-CoV-2 electrochemical biosensors is a miniaturized stainless steel acupuncture needle reported by Yang *et al.*[80] Compared to other electrochemical sensors, the small size and pinpoint nature of the acupuncture needle electrode was produced by successive deposition of AuNPs, rGO, poly (methylene blue) (PMB), and poly(ionic liquid)s. The specificity and stability of the sensor were tested using versatile biomolecules, such as bovine serum albumin (BSA), immunoglobulin G (IgG), immunoglobulin M (IgM), glutathione (GSH), and L-tryptophan (L-Trp), along with SARS-CoV-2-S protein for about 15 days. The same value after 7 days and 76% retention after 15 days indicate that the developed biosensor has high specificity and stability. Finally, a 38 pg mL^{-1}

LOD is the lowest sensitivity compared to the molecularly imprinted biosensors prior to January 2023. Jaewjaroenwattana *et al.*[81] reported a graphene ink printed on a disposable paper substrate as an electrochemical platform for the detection of SARS-CoV-2. Surprisingly, the three-electrode system sensor incorporated a cheap Whatman filter paper and a cost-effective plant-based anti-SARS-CoV-2 monoclonal antibody. The antibody was directly immobilized on the graphene-inked working electrode surface through covalent bonding. The electrochemical detection of the spike protein of SARS-CoV-2 was performed using a DPV. Consequently, the screen-printed sensor produced 2.0 fg mL^{-1} LOD with high specificity. Similarly, a metal graphene hybridized (*e.g.* ZnS/G) ultrasensitive electrochemical biosensor for the rapid detection of SARS-COV-2 was developed by Sarwar *et al.*[78] The nanocomposite sensor was fabricated by employing a step microwave-based non-equilibrium heating route on the glassy carbon electrode. Based on the previous electrochemical measurements in the testbed of biosensors, the LOD was 4.453×10^{-20} M for the synthetic DNA and 4.453×10^{-20} M for the SARS-CoV-2 standard, respectively.

Field-effect transistor (FET) biosensors

Field effect transistor (FET) biosensors are very widely used, highly sensitive,[70] ease to handle, and robust[87,88] compared to other techniques in the detection of the SARS-CoV-2 pandemic/epidemic. Versatile FETs, such as metal oxide semiconductor FET,[89] metal nanowire FET,[90] and disposable modular transistors,[91,92] have been reported as effective biosensors for the detection of SARS-CoV-2. Among these FETs, the graphene-based FET biosensors exhibited excellent electrocatalytic activity for high-sensitivity detection attributed to the unique physical, chemical, and electrical properties of graphene materials.[82,93] Particularly, the graphene-functionalized surface provides a suitable antibody–antigen immobilization environment and builds an amplified capacitance between bio-receptors and transducers.[72,94,95] Convincingly, the immobilized single-stranded DNA (ssDNA) on the graphene surface serves as a macromolecular antibody for detecting the SARS-COV-2 antigen. These interactions between the ssDNA-functionalized graphene and the SARS-COV-2 RNA may shift in Dirac voltage (*i.e.*, the minimum current point in the plot of I_{DS} *vs.* V_G, where I_{DS} is the drain current and V_G is the gate voltage) during the operation of graphene-based FET.[96] In addition to the experimental advancement, Toral-Lopez *et al.*[97] proposed a multi-scale simulation approach on graphene-based biological (Bio) FET. The author was motivated to carry out the study from the perspective that the Bio-FET takes advantage of other devices because the gate metal can detect minute amounts of ions or biomolecules. During the simulation, a single-layered graphene channel was mounted on top of the Si/SiO_2 layers, and then the complex formation between the human Angiotensin Converting Enzyme 2 (ACE2) and the virus spike protein S1 receptor binder domain (S1RBD) was investigated as a function of the Bio-FET. Employing a self-consistent simulation, the quantitative and qualitative sensitivity variation across different charge distribution zones (Dirac voltage, p-branch and n-branch) was observed by detecting ACE2-S1RBD using the graphene-based Bio-FET. The maximum current output from an *n*-branch belongs to the positive bias voltage in the Bio-FET.[97] However, both the utilization of unfunctionalized pristine graphene and the inconsiderate incubation condition of the virus are the partial limitations of this theoretical study.

Fig. 4a displays the schematic DNA aptamer-conjugated graphene-based FET sensor platform for the ultrasensitive detection of SARS-CoV-2 and its variants using patient samples.[99] As shown in Fig. 4b, when the SARS-CoV-2 virus was detected by the antibody of FET, the Dirac voltage (p- to n-channel transition point) is shifted to the right direction in the I_{DS} *vs.* V_G transfer curve, indicating that the electron concentrations are reduced at the graphene-sample fluid interface through the binding between antibody (DNA aptamer) and antigen (SARS-CoV-2). Fig. 3c shows the output characteristics (I_{DS} *vs.* V_{DS}, where V_{DS} is the drain voltage) of the graphene-based FET with an increasing negative voltage of V_G (*i.e.*, hole induction at the p-channel). When $V_G = 0$, there is a linear increase in I_{DS} as V_{DS} increases, indicating that there are free carriers at the graphene-sample interface (due to the zero bandgap effect). The shift of Dirac voltage (ΔV_G) was tested for the different variants of SARS-CoV-2. As a result, Fig. 4e demonstrates that ΔV_G is dependent on the species of the virus variant. Finally, Fig. 4f summarizes the sensing mechanism of graphene-based FET biosensors.[99] However, it is notable that graphene (*zero bandgap semiconductor*) exhibits a special behavior when employed as an FET channel layer. It shows a transition from the *p*-channel to the *n*-channel, *i.e.*, ambipolar behavior,[100,101] as shown in Fig. 4b. In addition, the output characteristic curve does not show a saturation but rather a linear increase even at $V_G = 0$ (Fig. 4c), indicating that the functionalized graphene is in a charge-doped state. Comparatively, it is notable that the organic semiconductor (*e.g.*, π-conjugated small molecules and polymers) shows a threshold voltage (V_{th}) in the transfer curve after filling the trap states at the semiconductor-insulator interface.[102,103] In addition, the charge mobility (μ) could be easily estimated using a FET testbed according to the following equations:

$$I_{DS} = \frac{1}{2}\mu C \frac{W}{L}(V_G - V_{th})V_{DS}, \quad (2)$$

$$I_{DS} = \frac{1}{2}\mu C \frac{W}{L}(V_G - V_{th})^2, \quad (3)$$

where C is the capacitance per unit area of the semiconductor/insulator/gate, W is channel width and L is channel length. Eqn (2) and (3) correspond to the linear and saturated regimes, respectively. Specifically, from the transconductance $g_m = (\delta I_{DS}/\delta V_G) = \mu C V_{DS} \cdot W/L$ in the transfer curve, the mobility can be calculated. Finally, it is worth remembering that (1) FET is a capacitor in which the charge concentration is a func-

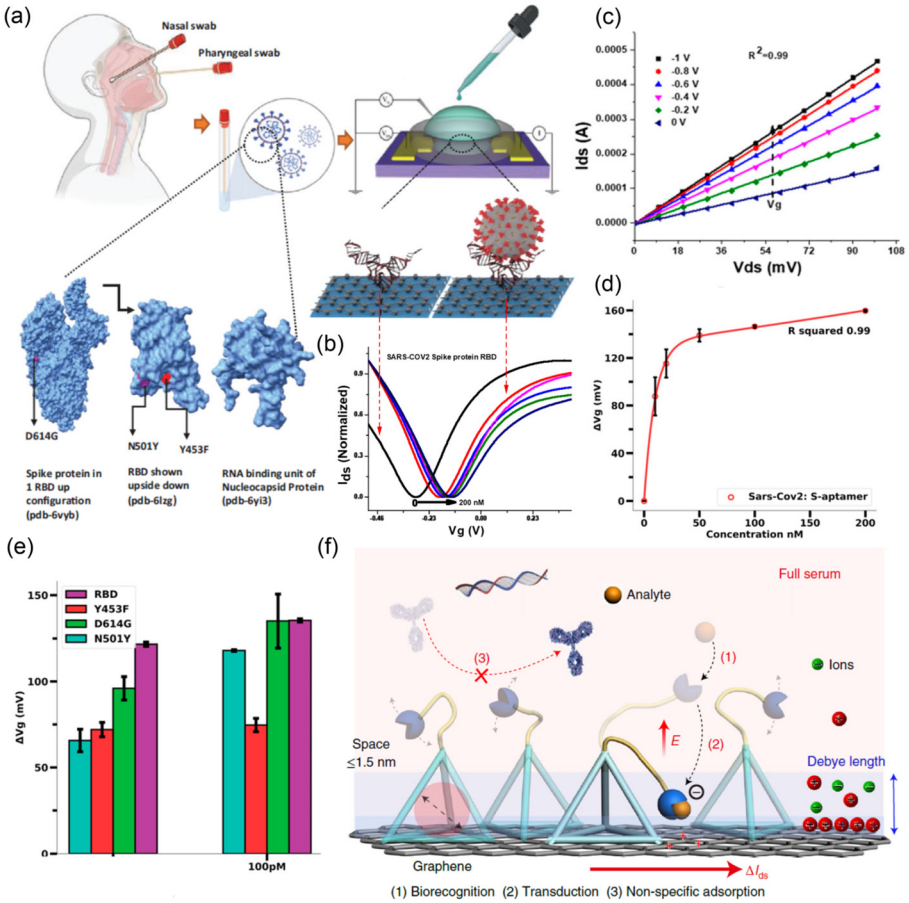

Fig. 4 (a) Schematic aptamer graphene-based FET sensor diagnostic system for ultrasensitive detection of SARS-CoV-2 using patient samples. (b) SARS-CoV-2 receptor-binding domain-mediated transfer curve analysis of Aptamer-S derivatized graphene-based FET. (c) Output characteristics (I_{DS} *vs.* V_{DS}) of graphene FET derivatized using 1-pyrenebutyric acid *N*-hydroxysuccinimide ester (PBASE, 5 mM) were analyzed by sweeping V_{GS} from 0 to 1 V at 0.2 V steps and variable drain source voltage (V_{DS}) of 0 to 100 mV with incremental steps of 10 mV. (d) Receptor-binding domain concentration (0 to 200 nM)-dependent sensor response on the Aptamer-S-derivatized FET. (e) Aptamer-S-derivatized graphene-based FET sensors were able to detect the B.1.1.7 variant (N501Y), mink-related mutation (Y453F), and mutation at the S2 domain (D614G) of SARS-Cov-2. (Reprinted[98] from *PNAS*). (f) Sensing mechanism of graphene-based FET biosensors. Owing to their high coverage of the surface, rigid bases avoid non-specific adsorption. The probes on the flexible cantilevers specifically recognize the targets. During electrostatic actuation, recognition events are detected in the g-FET channel, leading to efficient biorecognition and signal transduction. (Reprinted[99] from Nature Biomedical Engineering.)

tion of the applied gate voltage and the dielectric constant of the gate-insulator and that (2) the induced charge flow (*i.e.*, drift current) is modulated by the applied drain voltage. These two events mainly occur at the interface of the semiconductor-insulator (*e.g.*, graphene-patient sample), resulting in eqn (2) and (3). Hence, by sensing the graphene-sample interfacial difference, FET biosensors can detect the SARS-CoV-2 virus through antibody–antigen binding interaction.[98,99]

Interestingly, Seo *et al.*[71] fabricated a FET-based biosensor in which the SARS-CoV-2 spike 'antibody' is functionalized to a graphene sheet. The FET device could rapidly detect the cultured and nasopharyngeal swab specimens from SARS-CoV-2 patients at low concentrations of 1 fg mL^{-1} in PBS. Further, the FET biosensor detected SARS-CoV-2 in both culture medium and clinical samples with LOD: 1.6×10^1 plaque-forming unit (pfu) mL^{-1} and 2.42×10^2 copies per mL, respectively.[71] Another real-time SARS-CoV-2 detection *via* GO-based FET biosensors decorated with bimetallic platinum and palladium (Pt/Pd) nanoparticles was reported by Wasfi *et al.*[74] The authors underlined that the 'magnetic' spike antibody is useful to increase the sensitivity of SARS-CoV-2 antigen detection. Here, the FET device with the GO channel creates a suitable surface for the direct immobilization of specific antibodies against the SARS-CoV-2 spike protein. The high sensitivity with an LOD of up to 1 fg mL^{-1} towards the SARS-CoV-2 antigen in phosphate buffered saline (PBS) indicates the high performance of this FET biosensor for SARS-CoV-2 diagnosis.

Surface plasmon resonance biosensors

The surface plasmon resonance (SPR) sensor is an optical sensor,[104,105] affording rapid detection, accuracy, high sensi-

tivity, and portability.[106,107] The light source[108] and geometric configuration[109] are the governing criteria for SPR sensors. Commonly, the performances of SPR sensors are evaluated using the following equations:

$$S = \frac{\Delta\theta_r}{\Delta n_S}, \quad (4)$$

where S is the bulk refractive index (RI) sensitivity, $\Delta\theta_r$ is the change in the resonance angle and Δn_S is the change in the refractive index of the analyte. The important parameters in the resonance sensors are the small changes in the RI measurements, and the lowest-quantity detection is defined as follows:

$$\text{FOM} = \frac{S}{\text{FWHM}}, \quad (5)$$

where FOM is the figure of merit and FWHM is the full-width at half-maximum of the resonance spectrum.

$$\text{LOD} = m\frac{\sigma_{\text{blank}}}{S} \quad (6)$$

where m is a numerical factor (~2 or 3) and σ_{blank} is the standard deviation of the blank measures. Considering the aforementioned formality in the detection of the SARS-CoV-2 virus, the structure of SPR has been continually modified with different materials to enhance light absorption.[110] Recently, the graphene-based SPR sensors displayed a significant improvement in both detectivity and sensitivity towards SARS-CoV-2 based on the high light absorption coefficient and the 2D material's stability.[111,112]

For example, to increase light absorption for the detection of ultra-low SARS-COV-2, Hossain and Talukder[113] reported the analytical and numerical calculations of graphene-based SPR sensors by integrating them with tungsten disulfide (WS_2), potassium niobate ($KNbO_3$), black phosphorus (BP), and blue phosphorus (BlueP). In the Kretschmann configuration,[104] the positions of the incident light source, reflection and transmission detection planes for sensitivity characterization were simulated using a finite difference time domain (FDTD) technique. The sensor loaded with ACE-2 antibody on top of the plasmon sensor was in contact with a 1.70 nm thick graphene

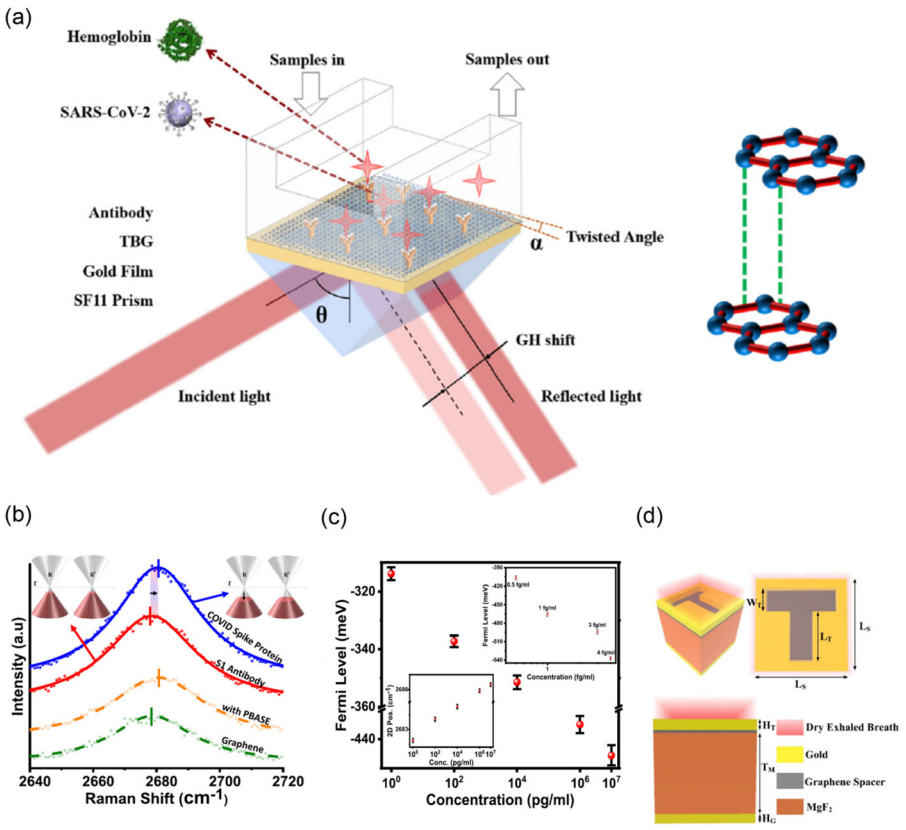

Fig. 5 (a) Schematic diagram of twisted bilayer graphene (TBG)-enhanced SPR biosensor. (Reprinted from publication[111] copyright @ 2023, with permission from DE GRUYTER.) (b) Depicted COVID spike protein detection *via* graphene phononics in PBS and 2D Raman peak of graphene (green), PBASE-modified graphene (orange), graphene-PBASE-antibody (red), and graphene-PBASE-antibody-spike protein (blue) structures and the attachment of PBASE p-dopes graphene, and the subsequent attachment of antibody n-dopes. (c) The 2D peak position (inset (bottom, left)) and the Fermi level of graphene change with various concentration ranges of the COVID spike protein in PBS. Similarly, the inset (top, right) shows the change in the Fermi level of graphene at low concentrations of spike protein in an artificial saliva medium. (Reprinted from[75] by the grant of the PMC Open Access Subset from ACS Nano.) (d) Refractive index sensor designed using a metasurface-based slotted T-shape perfect absorber (reprinted from publication[79] copyright @ 2022, with permission from Elsevier).

for both maximizing FWHM and reducing the R-profile. The designed sensor having stable binding kinetics towards loaded SARS-CoV-2 reached a LOD of 1 fM concentration (approximately 6×10^5 molecules) with a sensitivity of 201 degrees per RIU and 140 RIU-1 FOM. According to Hossain and Talukder,[113] the sensors could be useful for detecting SARS-CoV-2 and other biological samples. Similarly, Payandehpeyman *et al.*[114] developed graphene-based nanomechanical resonator sensors (*i.e.*, detecting a change in the mechanical response of the system when a foreign SARS-CoV-2 object is added) based on antibody–antigen interactions. For this simulation, the variables were the single-layer graphene sheet (SLGS) size, aspect ratio and boundary conditions, antibody concentration, and virus number variation. Accordingly, they measured the frequency shift and relative frequency. The result confirms that the simulated biosensor can detect SARS-CoV-2 with LOD 10 virus/test with high quality.[114] Captivatingly, the plasmonic-graphene biosensor with a four-layer configuration (Al, Au, SiO_2, and graphene) can detect SARS-CoV-2 with a sensitivity of 664.8 nm RIU^{-1} according to Negahdar *et al.*'s work.[115] In the case of Taya *et al.*'s contribution,[116] their SPR sensor is composed of three layers: Ag, $BiFeO_3$, and graphene. Here, the insertion of $BiFeO_3$ into the layered structure affords not only a high refractive index and low loss but also an extremely high sensitivity of 293 deg RIU^{-1}.

Du *et al.*[117] developed a tunable plasmonic biosensor using a 2D-twisted bilayer graphene superlattice on top of the plasmonic Au layer (Fig. 5a) that can produce an ultralow reflectivity of 2.2038×10^{-9} and large Goos–Hänchen (GH) shift of 4.4785×10^4 μm. For a fixed RI variation of 0.0012 RIU, the device with 44 nm AU and 55.3° twisted bilayer graphene could produce a high GH sensitivity of 3.9570×10^7 μm RIU^{-1}, affording the detection of 2.0 nM SARS-CoV-2 *via* a linear variation of 3×10^{-7} RIU.

Nguyen *et al.*[75] reported a SARS-CoV-2 spike protein-induced phononic modification in antibody-coupled graphene for viral detection applications. In their work (Fig. 5b), graphene, 1-pyrenebutanoic acid succinimidyl ester (PBASE)-modified graphene, graphene-PBASE-antibody, and graphene PBASE-antibody-spike protein phononic were studied using Raman spectroscopy as a detection platform. In all cases, the sensitivity is determined based on the change in the graphene 2D-phononic vibrational mode. As shown in Fig. 5b, after coupling the spike protein on the graphene PBASE, a blue shift on the 2D peak as a result of the p-doping of graphene was observed. This phenomenon can be directly correlated with the change in the Fermi level of graphene by p-doping. Consequently, the sensor's sensitivity (Fig. 5c) was measured by the shift in the Fermi level as a function of SARS-CoV-2 spike protein concentrations in phosphate-buffered saline (PBS). The chemio-phononic system can be detected at LODs of ~1 fg mL^{-1} in PBS and ~3.75 fg mL^{-1} in artificial saliva (see Table 1). The authors suggested that their detection method could be further modified to diagnose other COVID viral variants and diseases.

Furthermore, Patel *et al.*[79] proposed a novel refractive index sensor (RIS) for the detection of ethyl butanoate ($CH_3CH_2CH_2COOCH_2CH_3$) arising from the exhaled breath of SARS-CoV-2-infected persons, which is based on graphene's characteristics, such as its high surface area and easy functionalization. Fig. 5d shows the metasurface-based slotted T-shape perfect absorber RIS with a configuration of Au/MgF_2/graphene/Au. Finally, they obtained the highest sensitivity of 2500 nm RIU^{-1} with an LOD of 0.0224 RIU when the concentration of exhaled breath of SARS-CoV-2 was changed.

Conclusions and perspectives

Herein, we briefly reviewed the recent progress on graphene-based biosensors (*e.g.*, electrochemical, FET, and SPR) with the function of recognition and transduction for detecting the SARS-CoV-2 target. Compared to the current *polymerase chain reaction* (PCR) test for COVID-19, the aforementioned methods have a huge potential to provide a rapid, accurate and simple detection at low cost. Furthermore, these new diagnostic methods can secure a point-of-care (POC) platform, also called near-patient testing, to control the spread of the variant SARS-CoV-2 virus. For this purpose, if biosensors were integrated into portable devices, such as smartphones and wearable watches, it would result in real-time SARS-CoV-2 detection as an ideal scenario. Apparently, graphene with a 2D-hexagonal honeycomb lattice is believed to play an important role in this sensor technology. However, its special characteristics, such as 2D (a limited surface area) and zero bandgap (the presence of free charge carriers, as in doped semiconductors), could simultaneously act as some disadvantages. Hence, for further improving the sensitivity of graphene-based biosensors, the 2D/3D nanostructural control on top of the 2D-graphene layer should be recommended. To this end, a gold (Au) nanoparticular structure with a high surface area should be continuously useful for sufficiently functionalizing antibodies (*e.g.*, ssDNA aptamer), detecting SARS-CoV-2 targets through specific affinity by forming an antibody–antigen complex. Finally, the R&D activities, both experimental and theoretical, for eventual mass-production of biosensors with low cost, stability and high performance, should be continued in this post-pandemic era to tackle the coronavirus-like infectious disease in the future.

Conflicts of interest

The authors declare no competing financial interest.

Acknowledgements

The project (EDCF L/A No. ETH-6) entitled "Establishment of Centers of Excellence for Adama Science and Technology University" through international collaboration between Ethiopia and South Korea is appreciated.

References

1 J. P. A. Ioannidis, *Eur. J. Clin. Invest.*, 2020, **50**, e13423.
2 E. Morales-Narváez and C. Dincer, *Biosens. Bioelectron.*, 2020, **163**, 112274.
3 T. S. Fung and D. X. Liu, *Annu. Rev. Microbiol.*, 2019, **73**, 529–557.
4 H. A. Rothan and S. N. Byrareddy, *J. Autoimmun.*, 2020, **109**, 102433.
5 Y. Fan, K. Zhao, Z.-L. Shi and P. Zhou, *Viruses*, 2019, **11**, 210.
6 Z. Huang, D. Tian, Y. Liu, Z. Lin, C. J. Lyon, W. Lai, D. Fusco, A. Drouin, X. Yin, T. Hu and B. Ning, *Biosens. Bioelectron.*, 2020, **164**, 112316.
7 G. A. Naikoo, F. Arshad, I. U. Hassan, T. Awan, H. Salim, M. Z. Pedram, W. Ahmed, V. Patel, A. S. Karakoti and A. Vinu, *Bioeng. Transl. Med.*, 2022, **7**, e10305.
8 E. Borberg, E. Granot and F. Patolsky, *Nat. Commun.*, 2022, **13**, 6375.
9 X. Chen, Y. Liu, X. Zhan, Y. Gao, Z. Sun, W. Wen and W. Zheng, *Bioengineered*, 2022, **9**, 548.
10 D. M. Nguyen and T. T. T. Toan, *ECS Sens. Plus*, 2002, **1**, 031603.
11 Y. Gogotsi and B. Anasori, *ACS Nano*, 2019, **13**, 8491–8494.
12 M. Jaishankar, T. Tseten, N. Anbalagan, B. B. Mathew and K. N. Beeregowda, *Interdiscip. Toxicol.*, 2014, **7**, 60–72.
13 P. B. Tchounwou, C. G. Yedjou, A. K. Patlolla and D. J. Sutton, *Exper. Suppl.*, 2012, **101**, 133–164.
14 C.-W. Wang, C. Liang and H.-J. Yeh, *Chemosphere*, 2016, **147**, 82–87.
15 X. Wu, H. Zhang, J. Zhang and X. W. Lou, *Adv. Mater.*, 2021, **33**, 2008376.
16 Y. Wang, Z. Li, J. Wang, J. Li and Y. Lin, *Trends Biotechnol.*, 2011, **29**, 205–212.
17 S. Di, Y. Qian, L. Wang and Z. Li, *J. Mater. Sci.*, 2022, **57**, 3085–3113.
18 V. Georgakilas, M. Otyepka, A. B. Bourlinos, V. Chandra, N. Kim, K. C. Kemp, P. Hobza, R. Zboril and K. S. Kim, *Chem. Rev.*, 2012, **112**, 6156–6214.
19 C. Liao, Y. Li and S. C. Tjong, *Int. J. Mol. Sci.*, 2018, **19**, 3564.
20 S. Syama and P. V. Mohanan, *Int. J. Biol. Macromol.*, 2016, **86**, 546–555.
21 V. Palmieri and M. Papi, *Nano Today*, 2020, **33**, 100883.
22 S. J. Updike and G. P. Hicks, *Nature*, 1967, **214**, 986–988.
23 F. Maddalena, M. J. Kuiper, B. Poolman, F. Brouwer, J. C. Hummelen, D. M. d. Leeuw, B. D. Boer and P. W. M. Blom, *J. Appl. Phys.*, 2010, **108**, 124501.
24 J. D. Yuen, A. S. Dhoot, E. B. Namdas, N. E. Coates, M. Heeney, I. McCulloch, D. Moses and A. J. Heeger, *J. Am. Chem. Soc.*, 2007, **129**, 14367–14371.
25 L. G. Kaake, Y. Zou, M. J. Panzer, C. D. Frisbie and X.-Y. Zhu, *J. Am. Chem. Soc.*, 2007, **129**, 7824–7830.
26 V. M. C. H. Dias, A. F. Oliveira, A. K. B. B. Marinho, C. E. D. Santos Ferreira, C. E. F. Domingues, C. M. C. B. Fortaleza, C. F. D. L. Vidal, C. M. D. M. Carrilho, D. O. B. P. Pinheiro, D. B. de Assis, E. A. Medeiros, K. M. L. Morejón, L. Weissmann, L. Michelin, M. Carneiro, M. D. S. P. Nogueira, P. R. D. de Oliveira, R. J. Buralli, R. S. B. Stucchi, R. S. Lins, S. F. Costa and A. Chebabo, *Braz. J. Infect. Dis.*, 2022, **26**, 102703.
27 K. Alyafei, R. Ahmed, F. F. Abir, M. E. H. Chowdhury and K. K. Naji, *Comput. Biol. Med.*, 2022, **149**, 106070.
28 J. Sengupta and C. M. Hussain, *Inorganics*, 2023, **11**, 197.
29 C. S. Feldkamp and J. L. Carey, in *Immunoassay*, ed. E. P. Diamandis and T. K. Christopoulos, Immunoassay, Academic Press, San Diego, CA, USA, 1996, pp. 5–24.
30 C. C. Smith, K. S. Olsen, K. M. Gentry, M. Sambade, W. Beck, J. Garness, S. Entwistle, C. Willis, S. Vensko, A. Woods, M. Fini, B. Carpenter, E. Routh, J. Kodysh, T. O'Donnell, C. Haber, K. Heiss, V. Stadler, E. Garrison, A. M. Sandor, J. P. Y. Ting, J. Weiss, K. Krajewski, O. C. Grant, R. J. Woods, M. Heise, B. G. Vincent and A. Rubinsteyn, *Genome Med.*, 2021, **13**, 101.
31 M. F. Bachmann, M. O. Mohsen, L. Zha, M. Vogel and D. E. Speiser, *npj Vaccines*, 2021, **6**, 2.
32 C. Rosadas, M. Khan, E. Parker, F. Marchesin, K. Katsanovskaja, M. Sureda-Vives, N. Fernandez, P. Randell, R. Harvey, A. Lilley, B. H. L. Harris, M. Zuhair, M. Fertleman, S. Ijaz, S. Dicks, C.-E. Short, R. Quinlan, G. P. Taylor, K. Hu, P. McKay, A. Rosa, C. Roustan, M. Zuckerman, K. El Bouzidi, G. Cooke, B. Flower, M. Moshe, P. Elliott, A. J. Spencer, T. Lambe, S. C. Gilbert, H. Kingston, J. K. Baillie, P. J. M. Openshaw, M. G. Semple, P. Cherepanov, M. O. McClure and R. S. Tedder, *J. Virol. Methods*, 2022, **302**, 114475.
33 L. B. Shrestha, N. Tedla and R. A. Bull, *Front. Immunol.*, 2021, **12**, 752003.
34 L. Min and Q. Sun, *Front. Mol. Biosci.*, 2021, **8**, 671633.
35 M. Fukuda, M. S. Islam, R. Shimizu, H. Nasser, N. N. Rabin, Y. Takahashi, Y. Sekine, L. F. Lindoy, T. Fukuda, T. Ikeda and S. Hayami, *ACS Appl. Nano Mater.*, 2021, **4**, 11881–11887.
36 M. I. Katsnelson, *Mater. Today*, 2007, **10**, 20–27.
37 C. N. R. Rao, K. Biswas, K. S. Subrahmanyam and A. Govindaraj, *J. Mater. Chem.*, 2009, **19**, 2457–2469.
38 G. Yang, L. Li, W. B. Lee and M. C. Ng, *Sci. Technol. Adv. Mater.*, 2018, **19**, 613–648.
39 C. Soldano, A. Mahmood and E. Dujardin, *Carbon*, 2010, **48**, 2127–2150.
40 P. Avouris and C. Dimitrakopoulos, *Mater. Today*, 2012, **15**, 86–97.
41 C. N. R. Rao, A. K. Sood, R. Voggu and K. S. Subrahmanyam, *J. Phys. Chem. Lett.*, 2010, **1**, 572–580.
42 M. B. Burkholder, F. B. A. Rahman, E. H. Chandler, J. R. Regalbuto, B. F. Gupton and J. M. M. Tengco, *Carbon Trends*, 2022, **9**, 100196.
43 B. Aïssa, N. K. Memon, A. Ali and M. K. Khraisheh, *Front. Mater.*, 2015, **2**, 58.
44 Y. Duan, C. D. Stinespring and B. Chorpening, *ChemistryOpen*, 2015, **4**, 642–650.

45 P. Tian, L. Tang, K. S. Teng and S. P. Lau, *Mater. Today Chem.*, 2018, **10**, 221–258.
46 R. Zan, A. Altuntepe and S. Erkan, *Phys. E*, 2021, **128**, 114629.
47 H. Rasuli, R. Rasuli, M. Alizadeh and G. BoonTong, *Results Phys.*, 2020, **18**, 103200.
48 P.-C. Lin, R. Villarreal, S. Achilli, H. Bana, M. N. Nair, A. Tejeda, K. Verguts, S. De Gendt, M. Auge, H. Hofsäss, S. De Feyter, G. Di Santo, L. Petaccia, S. Brems, G. Fratesi and L. M. C. Pereira, *ACS Nano*, 2021, **15**, 5449–5458.
49 F. Hadish, M.-H. Chiang, Y.-F. Hsieh, S.-Y. Wu and S. Jou, *Adv. Mater. Sci. Eng.*, 2022, **2022**, 4574772.
50 D. R. Yanti, U. Hikmah, A. Prasetyo and E. Hastuti, *IOP Conf. Ser.: Earth Environ. Sci.*, 2020, **456**, 012008.
51 M. Lee and S.-M. Paek, *Nanomaterials*, 2022, **12**, 1507.
52 F. Hadish, S. Jou, B.-R. Huang, H.-A. Kuo and C.-W. Tu, *J. Electrochem. Soc.*, 2017, **164**, B336.
53 J. H. Jeong, S. Kang, N. Kim, R. Joshi and G.-H. Lee, *Phys. Chem. Chem. Phys.*, 2022, **24**, 10684–10711.
54 C. Sainz-Urruela, S. Vera-López, M. Paz San Andrés and A. M. Díez-Pascual, *J. Mol. Liq.*, 2022, **357**, 119104.
55 Z. Guo, S. Chakraborty, F. A. Monikh, D.-D. Varsou, A. J. Chetwynd, A. Afantitis, I. Lynch and P. Zhang, *Adv. Biol.*, 2021, **5**, 2100637.
56 D. Chen, H. Feng and J. Li, *Chem. Rev.*, 2012, **112**, 6027–6053.
57 D. A. Dikin, S. Stankovich, E. J. Zimney, R. D. Piner, G. H. B. Dommett, G. Evmenenko, S. T. Nguyen and R. S. Ruoff, *Nature*, 2007, **448**, 457–460.
58 K. Chaudhary, K. Kumar, P. Venkatesu and D. T. Masram, *Adv. Colloid Interface Sci.*, 2021, **289**, 102367.
59 M. K. Rabchinskii, S. A. Ryzhkov, N. A. Besedina, M. Brzhezinskaya, M. N. Malkov, D. Y. Stolyarova, A. F. Arutyunyan, N. S. Struchkov, S. D. Saveliev, I. D. Diankin, D. A. Kirilenko, S. I. Pavlov, D. V. Potorochin, F. Roth, M. V. Gudkov, A. A. Gulin, P. Cai, Z. Liu, A. V. Golovin and P. N. Brunkov, *Carbon*, 2022, **196**, 264–279.
60 F. Wang, L. Liu and W. J. Li, *IEEE Trans. NanoBiosci.*, 2015, **14**, 818–834.
61 C. Zhang, Z. Zhang, Q. Yang and W. Chen, *Electroanalysis*, 2018, **30**, 2504–2524.
62 M. T. Hwang, M. Heiranian, Y. Kim, S. You, J. Leem, A. Taqieddin, V. Faramarzi, Y. Jing, I. Park, A. M. van der Zande, S. Nam, N. R. Aluru and R. Bashir, *Nat. Commun.*, 2020, **11**, 1543.
63 Y. Bai, T. Xu and X. Zhang, *Micromachines*, 2020, **11**, 60.
64 A. Balaji, S. Yang, J. Wang and J. Zhang, *Biosensors*, 2019, **9**, 74.
65 J. Lee, K. Takemura and E. Y. Park, *Sens. Actuators, B*, 2018, **276**, 254–261.
66 K. Navakul, C. Sangma, P.-t. Yenchitsomanus, S. Chunta and P. A. Lieberzeit, *Anal. Bioanal. Chem.*, 2021, **413**, 6191–6198.
67 R. Dutta, K. Rajendran, S. K. Jana, L. M. Saleena and S. Ghorai, *Biosensors*, 2023, **13**, 349.
68 S. Afsahi, M. B. Lerner, J. M. Goldstein, J. Lee, X. Tang, D. A. Bagarozzi, D. Pan, L. Locascio, A. Walker, F. Barron and B. R. Goldsmith, *Biosens. Bioelectron.*, 2018, **100**, 85–88.
69 T. Ando, *NPG Asia Mater.*, 2009, **1**, 17–21.
70 S. Yasri and V. Wiwanitkit, *Sens. Int.*, 2022, **3**, 100171.
71 G. Seo, G. Lee, M. J. Kim, S.-H. Baek, M. Choi, K. B. Ku, C.-S. Lee, S. Jun, D. Park, H. G. Kim, S.-J. Kim, J.-O. Lee, B. T. Kim, E. C. Park and S. I. Kim, *ACS Nano*, 2020, **14**, 5135–5142.
72 Y. Li, Z. Peng, N. J. Holl, M. R. Hassan, J. M. Pappas, C. Wei, O. H. Izadi, Y. Wang, X. Dong, C. Wang, Y.-W. Huang, D. Kim and C. Wu, *ACS Omega*, 2021, **6**, 6643–6653.
73 B. V. Krsihna, S. Ahmadsaidulu, S. S. T. Teja, D. Jayanthi, A. Navaneetha, P. R. Reddy and M. D. Prakash, *Silicon*, 2022, **14**, 5913–5921.
74 A. Wasfi, F. Awwad, N. Qamhieh, B. Al Murshidi, A. R. Palakkott and J. G. Gelovani, *Sci. Rep.*, 2022, **12**, 18155.
75 N. H. L. Nguyen, S. Kim, G. Lindemann and V. Berry, *ACS Nano*, 2021, **15**, 11743–11752.
76 T. Beduk, D. Beduk, J. I. de Oliveira Filho, F. Zihnioglu, C. Cicek, R. Sertoz, B. Arda, T. Goksel, K. Turhan, K. N. Salama and S. Timur, *Anal. Chem.*, 2021, **93**, 8585–8594.
77 S. Kim, H. Ryu, S. Tai, M. Pedowitz, J. R. Rzasa, D. J. Pennachio, J. R. Hajzus, D. K. Milton, R. Myers-Ward and K. M. Daniels, *Biosens. Bioelectron.*, 2022, **197**, 113803.
78 S. Sarwar, M.-C. Lin, C. Amezaga, Z. Wei, E. Iyayi, H. Polk, R. Wang, H. Wang and X. Zhang, *Adv. Compos. Hybrid Mater.*, 2023, **6**, 49.
79 S. K. Patel, J. Surve, J. Parmar, K. Aliqab, M. Alsharari and A. Armghan, *Diamond Relat. Mater.*, 2023, **132**, 109644.
80 X. Yang, Z.-Z. Yin, G. Zheng, M. Zhou, H. Zhang, J. Li, W. Cai and Y. Kong, *Bioelectrochemistry*, 2023, **151**, 108375.
81 J. Jaewjaroenwattana, W. Phoolcharoen, E. Pasomsub, P. Teengam and O. Chailapakul, *Talanta*, 2023, **251**, 123783.
82 T. Ji, Z. Liu, G. Wang, X. Guo, S. Akbar khan, C. Lai, H. Chen, S. Huang, S. Xia, B. Chen, H. Jia, Y. Chen and Q. Zhou, *Biosens. Bioelectron.*, 2020, **166**, 112455.
83 F. Mollarasouli, S. Kurbanoglu and S. A. Ozkan, *Biosensors*, 2019, **9**, 86.
84 Z. Zhao, C. Huang, Z. Huang, F. Lin, Q. He, D. Tao, N. Jaffrezic-Renault and Z. Guo, *TrAC, Trends Anal. Chem.*, 2021, **139**, 116253.
85 M. Alafeet, K. Dighe, P. Moitra and D. Pan, *ACS Nano*, 2020, **14**, 17028–17045.
86 D. Sadighbayan, A. Minhas-Khan and E. Ghafar-Zadeh, *IEEE Trans. NanoBiosci.*, 2022, **21**, 232–245.
87 N. Alnaji, A. Wasfi and F. Awwad, *Sci. Rep.*, 2023, **13**, 4485.
88 N. H. Al-Hardan, M. Firdaus-Raih, M. A. A. Hamid and A. Jalar, *Crit. Rev. Solid State Mater. Sci.*, 2023, DOI: **10.1080/10408436.2023.2169657**.

89 M. T. Amen, T. T. Pham, E. Cheah, D. P. Tran and B. Thierry, *Molecules*, 2022, **27**, 7952.
90 A. Wasfi, F. Awwad, J. G. Gelovani, N. Qamhieh and A. I. Ayesh, *Nanomaterials*, 2022, **12**, 2638.
91 C.-W. Chiu, M. Xian, J. L. Stephany, X. Xia, C.-C. Chiang, F. Ren, C.-T. Tsai, S.-S. Shan, Y.-T. Liao, J. F. Esquivel-Upshaw, S. R. Rananaware, L. T. Nguyen, N. C. Macaluso, P. K. Jain, M. N. Cash, C. N. Mavian, M. Salemi, M. E. Leon, C.-W. Chang, J. Lin and S. J. Pearton, *J. Vac. Sci. Technol., B: Nanotechnol. Microelectron.: Mater., Process., Meas., Phenom.*, 2022, **40**, 023204.
92 C.-C. Chiang, C.-W. Chiu, F. Ren, C.-T. Tsai, Y.-T. Liao, J. F. Esquivel-Upshaw and S. J. Pearton, *J. Vac. Sci. Technol., B: Nanotechnol. Microelectron.: Mater., Process., Meas., Phenom.*, 2022, **41**, 012204.
93 S. Sreejith, J. Ajayan, J. M. Radhika, B. Sivasankari, S. Tayal and M. Saravanan, *Measurement*, 2023, **206**, 112202.
94 P. K. Sharma, E.-S. Kim, S. Mishra, E. Ganbold, R.-S. Seong, A. K. Kaushik and N.-Y. Kim, *ACS Sens.*, 2021, **6**, 3468–3476.
95 N. Alnaji, A. Wasfi and F. Awwad, *Sci. Rep.*, 2023, **13**, 4485.
96 I. Park, J. Lim, S. You, M. T. Hwang, J. Kwon, K. Koprowski, S. Kim, J. Heredia, S. A. Stewart de Ramirez, E. Valera and R. Bashir, *ACS Sens.*, 2021, **6**, 4461–4470.
97 A. Toral-Lopez, D. B. Kokh, E. G. Marin, R. C. Wade and A. Godoy, *Nanoscale Adv.*, 2022, **4**, 3065–3072.
98 D. K. Ban, T. Bodily, A. G. Karkisaval, Y. Dong, S. Natani, A. Ramanathan, A. Ramil, S. Srivastava, P. Bandaru, G. Glinsky and R. Lal, *Proc. Natl. Acad. Sci. U. S. A.*, 2022, **119**, e2206521119.
99 L. Wang, X. Wang, Y. Wu, M. Guo, C. Gu, C. Dai, D. Kong, Y. Wang, C. Zhang, D. Gu, C. Fan, Y. Xie, Z. Zhu, Y. Liu and D Wei, *Nat. Biomed. Eng.*, 2022, **6**, 276–285.
100 J. Y. Kim and C. D. Frisbie, Correlation of phase behavior and charge transport in conjugated polymer/fullerene blends, *J. Phys. Chem. C*, 2008, **112**, 17726–17736.
101 J. Y. Kim, H. Cho, S. Noh, Y. Lee, Y. M. Nam, C. Lee and W. H. Jo, Charge transport in amorphous low bandgap conjugated polymer/fullerene films, *J. Appl. Phys.*, 2012, **111**, 043710.
102 Z. Bao and J. Locklin, *Organic Field Effect Transistor*, CRC press, Boca Raton, FL, 2007.
103 A. J. Heeger, N. S. Sariciftci and E. B. Namdas, *Semiconducting and Metallic Polymers*, Oxford University Press, Oxford, UK, 2010.
104 E. Kretschmann and H. Raether, *Z. Naturforsch.*, 1968, **23a**, 2135–2136.
105 B. Liedberg, C. Nylander and I. Lunström, *Sens. Actuators*, 1983, **4**, 299–304.
106 B. A. Prabowo, A. Purwidyantri and K. C. Liu, *Biosensors*, 2018, **8**, 80.
107 W. Xiaoying, M. Mingqiang, W. Xueliang and W. Shoujuan, in *Analytical Chemistry*, ed. S. Abhay Nanda, IntechOpen, Rijeka, 2020, DOI: **10.5772/intechopen.92549**, p. Ch. 5.
108 J. Homola, *Chem. Rev.*, 2008, **108**, 462–493.
109 Q. Duan, Y. Liu, S. Chang, H. Chen and J.-h. Chen, *Sensors*, 2021, **21**, 5262.
110 P. S. Pandey, S. K. Raghuwanshi, A. Shadab, M. T. I. Ansari, U. K. Tiwari and S. Kumar, *IEEE Sens. J.*, 2022, **22**, 13800–13810.
111 T. B. Akib, S. F. Mou, M. M. Rahman, M. M. Rana, M. R. Islam, I. M. Mehedi, M. A. P. Mahmud and A. Z. Kouzani, *Sensors*, 2021, **21**, 3491.
112 S. Mostufa, T. B. A. Akib, M. M. Rana, I. M. Mehedi, U. M. Al-Saggaf, A. U. Alsaggaf, M. U. Alsaggaf and M. S. Alam, *Opt. Continuum.*, 2022, **1**, 494–515.
113 M. M. Hossain and M. A. Talukder, *PLoS One*, 2023, **18**, e0284812.
114 J. Payandehpeyman, N. Parvini, K. Moradi and N. Hashemian, *ACS Appl. Nano Mater.*, 2021, **4**, 6189–6200.
115 R. Negahdari, E. Rafiee and Z. Kordrostami, *Plasmonics*, 2023, **18**, 1325–1335.
116 S. A. Taya, M. G. Daher, A. H. M. Almawgani, A. T. Hindi, S. H. Zyoud and I. Colak, *Plasmonics*, 2023, **18**, 1441–1448.
117 F. Du, K. Zheng, S Zeng and Y. Yuan, *Nanophotonics*, 2023, **12**, 1271–1284.